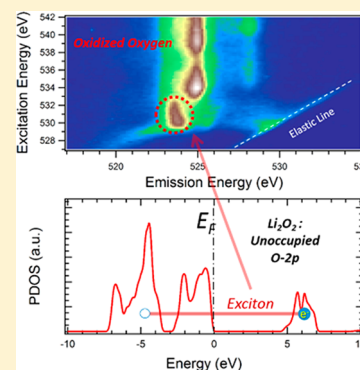


Spectroscopic Signature of Oxidized Oxygen States in Peroxides

Zengqing Zhuo,^{†,‡,⊥} Chaitanya Das Pemmaraju,^{§,⊥} John Vinson,^{||} Chunjing Jia,[§] Brian Moritz,[§] Ilkyu Lee,[§] Shawn Sallies,[‡] Qinghao Li,[‡] Jinpeng Wu,[‡] Kehua Dai,[‡] Yi-de Chuang,^{‡,⊥} Zahid Hussain,^{‡,⊥} Feng Pan,^{*,†,⊥} Thomas P. Devereaux,^{*,§} and Wanli Yang^{*,‡,⊥}[†]School of Advanced Materials, Shenzhen Graduate School, Peking University, Shenzhen 518055, People's Republic of China[‡]Advanced Light Source, Lawrence Berkeley National Laboratory, 1 Cyclotron Road, Berkeley California 94720, United States[§]Stanford Institute for Materials and Energy Sciences, Stanford University and SLAC National Accelerator Laboratory, Menlo Park, California 94025, United States^{||}Material Measurement Laboratory, National Institute of Standards and Technology, Gaithersburg, Maryland 20899, United States

Supporting Information

ABSTRACT: Recent debates on the oxygen redox behaviors in battery electrodes have triggered a pressing demand for the reliable detection and understanding of nondivalent oxygen states beyond conventional absorption spectroscopy. Here, enabled by high-efficiency mapping of resonant inelastic X-ray scattering (mRIXS) coupled with first-principles calculations, we report distinct mRIXS features of the oxygen states in Li_2O , Li_2CO_3 , and especially, Li_2O_2 , which are successfully reproduced and interpreted theoretically. mRIXS signals are dominated by valence-band decays in Li_2O and Li_2CO_3 . However, the oxidized oxygen in Li_2O_2 leads to partially unoccupied O-2p states that yield a specific intraband excitonic feature in mRIXS. Such a feature displays a specific emission energy in mRIXS, which disentangles the oxidized oxygen states from the dominating transition-metal/oxygen hybridization features in absorption spectroscopy, thus providing critical hints for both detecting and understanding the oxygen redox reactions in transition-metal oxide based battery materials.



Lithium peroxide, Li_2O_2 , has been an intriguing system for both structural and chemical properties related to its special oxygen states.¹ Technologically, Li_2O_2 is an important air purification agent in spacecraft because it is not hygroscopic as other peroxides and is highly reactive with CO_2 . Recently, the nondivalent oxygen state has attracted increased attention in electrochemical energy storage systems including both alkali-ion batteries and Li-air batteries.^{2,3} Li_2O_2 is one of the key reaction products in Li-air batteries.² Li_2O_2 , together with Li_2O and Li_2CO_3 , also dominates the inorganic components of the critical solid-electrolyte-interphase layer formed on negative electrodes of Li-ion batteries.^{4–6} More importantly, peroxides may be involved in redox reactions in transition-metal (TM) oxide based electrodes:^{3,7} a view that is challenged by other models.^{8,9}

The redox-active oxygen is a critical concept because conventional batteries rely on only TM redox reactions, and oxygen redox is potentially useful for improving the capacity and energy density of batteries.^{10,11} Additionally, oxygen redox could also impact the conceptual developments of catalytic materials.¹⁰ However, although it is widely believed now that oxygen in TM oxide based electrodes could be oxidized to nondivalent states during the electrochemical cycling, as indicated by various core-level X-ray spectroscopy and recent Compton scattering experiments,^{11,12} the nature of such an oxygen redox state has been under active debate,^{7–9} and the oxidized nondivalent oxygen remains to be understood and

reliably characterized.^{11,13} Therefore, a reliable and direct detection of the intrinsic oxygen state, as well as its theoretical understanding, has become crucial for both the fundamental understanding and practical developments of various electrochemical materials.

The challenge of detecting the unconventional oxygen states in TM oxides and the need for better characterizations stem from the fact that conventional O *K*-edge soft X-ray absorption spectroscopy (sXAS) involves entangled contributions through hybridizations between TMs and oxygen. To be more specific, O-*K* sXAS studies have shown that Li_2O_2 displays a characteristic broad feature around 530 to 532 eV in sXAS.¹⁴ Unfortunately, this broad feature is located in the same energy range where TM contributes significantly to the O-*K* sXAS “pre-edge” signals through hybridizations, as identified in the seminal work by de Groot et al. in 1989.¹⁵ Moreover, the overall broadening of the XAS line shape, due to the presence of a strong core hole created via absorption, often masks low-energy features that are relevant for understanding oxygen redox, complicating a simple interpretation. Indeed, we have recently clarified that most of the claims and conclusions on oxygen redox states based on sXAS experiments merely

Received: September 7, 2018

Accepted: October 16, 2018

Published: October 16, 2018



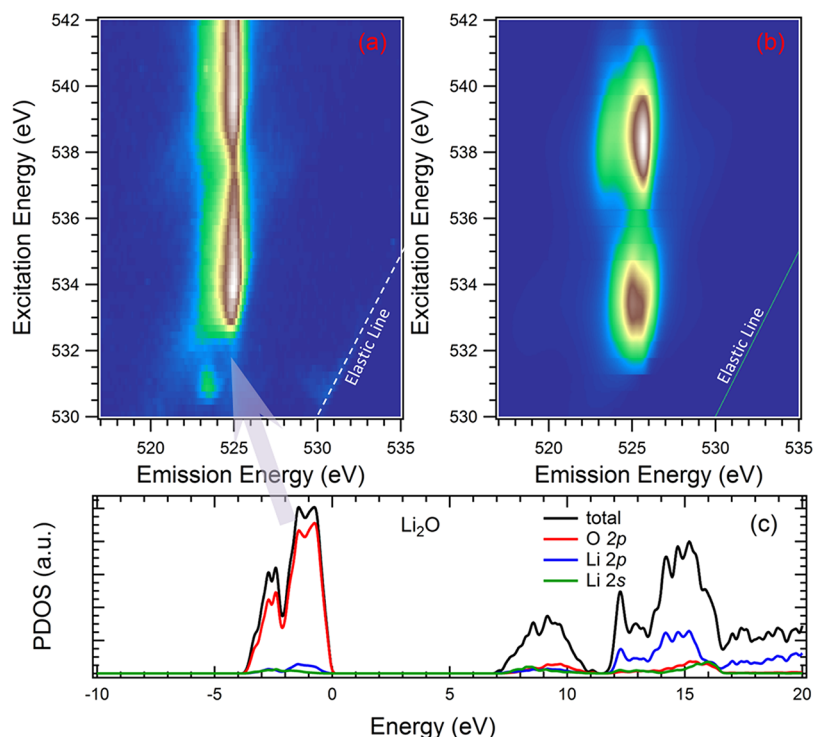


Figure 1. (a) Experimental O *K*-edge mRIXS of Li_2O , which is dominated by the emission feature around 525 eV emission energy. Color indicates the intensity distribution of the emitted photons, with blue presenting low intensity and white presenting high intensity. (b) Calculated mRIXS of Li_2O , which reproduce the dominate features shown in experimental results. (c) Total and projected density of states of Li_2O . The emission line in mRIXS is reproduced in mRIXS calculations by considering the decay of the valence band states, indicated by the arrow.

represent the change of TM states upon electrochemical cycling.¹³ An advanced characterization beyond conventional O-*K* sXAS with better elemental and chemical-bond sensitivity, as well as deeper probe depth, is urgently needed in order to detect and understand the intrinsic nature of oxygen states.

We have recently shown that high-efficiency full energy range mapping of resonant X-ray inelastic scattering (mRIXS) can successfully decipher the entangled O-*K* signals through the new dimension of information on emission photon energies.¹³ By covering the full excitation energy range of O-*K* sXAS, mRIXS detects the energy distribution curves of the fluorescence photons that is only counted as a single number in sXAS; i.e., mRIXS further resolves the emitted photons along the new dimension of emission energy at each absorption energy. Moreover, mRIXS does not suffer from core-hole broadening as in sXAS because the core-hole is filled in the final state of the RIXS process. mRIXS thus becomes a perfect tool-of-choice for reliable and conclusive studies of novel chemical states that cannot be resolved in sXAS.^{13,16–18} Strikingly, O-*K* mRIXS has revealed a sharp feature of the oxygen redox state in battery electrodes that has been buried in conventional sXAS data, with 531 eV excitation energy and 523 to 524 eV emission energy, clearly separated from the TM-O hybridization features at 525 eV emission energy.^{13,17,18}

However, while mRIXS has been established as a reliable probe of the critical oxygen states involved in the battery electrodes with oxygen redox activities, the interpretation of specific O-*K* mRIXS features has not yet been achieved. The experimental results of mRIXS involve complex processes that are related to electron state configurations, electron correlations, and excitations, which are challenging topics in both fundamental physics and spectroscopic simulations. In general,

signals in mRIXS could be categorized into three different types of contributions, the elastic line, nonresonant emission signals from the decays of the occupied valence band electrons to the core holes (“emission lines”), and low-energy excitations.¹³ While model compounds may not represent directly the same mechanism as in the complex TM oxide systems, a benchmark study with combined experimental and theoretical results becomes crucial for a general identification of the mRIXS observations, which will shed light on the understanding of the unusual oxygen states involved in the intense debates on TM oxide based energy materials.

In this work, we provide a combined experimental and theoretical mRIXS study of Li_2O_2 , Li_2O , and Li_2CO_3 . Our central goal is to detect and identify the nature of the aforementioned critical O-*K* mRIXS feature in Lithium peroxide, thus providing benchmarks and guidelines for understanding the O-*K* mRIXS findings in energy materials. We note that collecting reliable mRIXS data from Li_2O_2 is a nontrivial issue due to the typical low count rates of RIXS experiments and the radiation sensitivity of the material.^{14,19} These technical challenges have now been solved through our recently commissioned RIXS system with ultrahigh detection efficiency,^{20,21} and mRIXS results are successfully collected with controlled sample transfer, cooling, and rastering. Furthermore, advanced simulations with the OCEAN package^{22,23} are performed and compared directly with experimental results. We are able to identify the origins of the O-*K* mRIXS experimental features in all the three compounds. We found that mRIXS features of Li_2O and Li_2CO_3 are dominated by emission lines from the decays of valence-band electrons. However, a unique excitation feature is defined in Li_2O_2 which is a spectroscopic signature of nondivalent oxygen states. Since

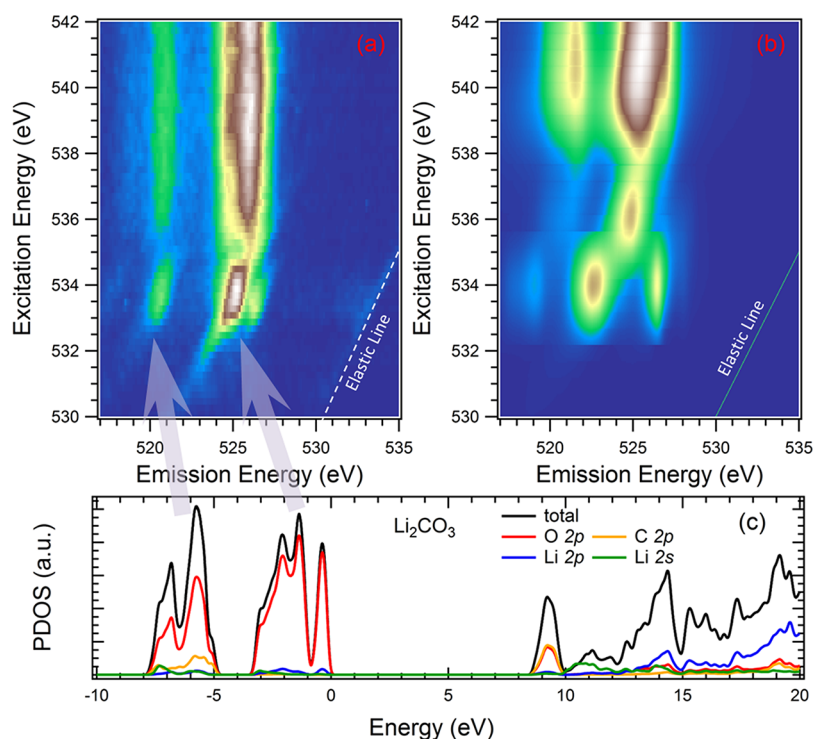


Figure 2. (a) Experimental O *K*-edge mRIXS of Li_2CO_3 . Two emission features centered at 521 and 526 eV emission energy are observed. (b) Calculated mRIXS of Li_2CO_3 successfully reproduces the experimental features by considering the emissions from the decay of the split valence band states, which are shown in part c.

such oxygen states have partially filled oxygen 2p bands, we found that the role of Coulomb correlations is critical in adjusting spectral weights. Our combined experimental and theoretical results for Li_2O_2 reveal and interpret the critical mRIXS feature at 523.5 eV emission energy across the 529 to 532.5 eV excitation energy, which represents a characteristic O-2p intraband excitation in peroxide materials. Strikingly, although much broader along excitation energies, this particular mRIXS feature is close to the observations of the sharp oxygen redox feature in TM oxide based battery materials,^{13,17,18} suggesting that the oxygen-redox mRIXS feature found in battery electrodes is intrinsically associated with the partially occupied O-2p bands in a highly oxidized TM oxide system.

mRIXS of Li_2O_2 , Li_2O , and Li_2CO_3 were collected at the high-efficiency iRIXS endstation of BL8.0.1 of the Advanced Light Source.^{20,24} Li_2O_2 is unstable under air exposure (forming Li_2CO_3), heating (decomposes at 450 °C to Li_2O), and X-ray excitations (both Li_2O_2 and Li_2CO_3 decompose to Li_2O).^{14,19} Therefore, despite the high detection efficiency that allows us to collect a full-range mRIXS map in only about 30 min, we employed extensive practices on sample transfer,^{25,26} liquid N_2 cooling, and sample scanning to reduce the radiation effects (see Supporting Information). Still, as elaborated below, some radiation effects remain in our Li_2O_2 data. However, comparative studies of all the three materials allow us to distinguish the contributions from material degradation. Additionally, sXAS studies show that Li_2O_2 slowly become Li_2O under irradiation,¹⁴ the distinct mRIXS features reported here indicate that the signals are intrinsic results of different materials.

First-principles simulations of mRIXS were carried out using the OCEAN package.^{22,23} Details of the RIXS implementation

within OCEAN have been described previously^{27,28} and briefly in Supporting Information. Experimentally determined cubic Li_2O ,²⁹ hexagonal Li_2O_2 ^{30,31} and monoclinic Li_2CO_3 ³² unit cell structures were used in the simulations. Exchange-correlation effects were treated at the LDA+*U* level with the Hubbard parameter set to $U = 6$ eV on O-2p and C-2p states, similar to previous reports.^{33,34} Other details on Brillouin zone, core-hole lifetime, photon polarizations, and adjustments of band gaps are available in the Supporting Information.

For the purpose of comparisons, we first present the mRIXS experiments and theoretical interpretation of Li_2O and Li_2CO_3 . Both have a formal valence of O^{2-} and a nominally fully occupied O-2p shell. We then focus on the specific feature of Li_2O_2 arising from its partially filled O-2p band.

The experimental mRIXS of Li_2O is shown in Figure 1a. Other than the elastic line, strong features around 525 eV emission energy (horizontal axis) dominate the whole map but are separated into two overall packets of intensity along excitation energy regimes, 533–536 and 539–542 eV (vertical axis). The outgoing photon's emission energy is independent of the incident excitation energy, indicating that these are fluorescence-like emission lines from the decay of electrons from valence bands (VBs) to the core holes.¹³ Indeed, the energy of this emission line is consistent with the X-ray emission spectra of Li_2O .¹⁹ The origin of the two regimes of excitation energies could be understood by comparing with the O-K sXAS spectrum (Figure S1). Consistent with the previous report,¹⁴ there are two broad absorption features observed for Li_2O . The excitation energy ranges of the two sXAS features are the same as those of the two mRIXS intensity packets, which naturally explains the two mRIXS portions from sXAS process, i.e., exciting electrons from the O 1s core level to the

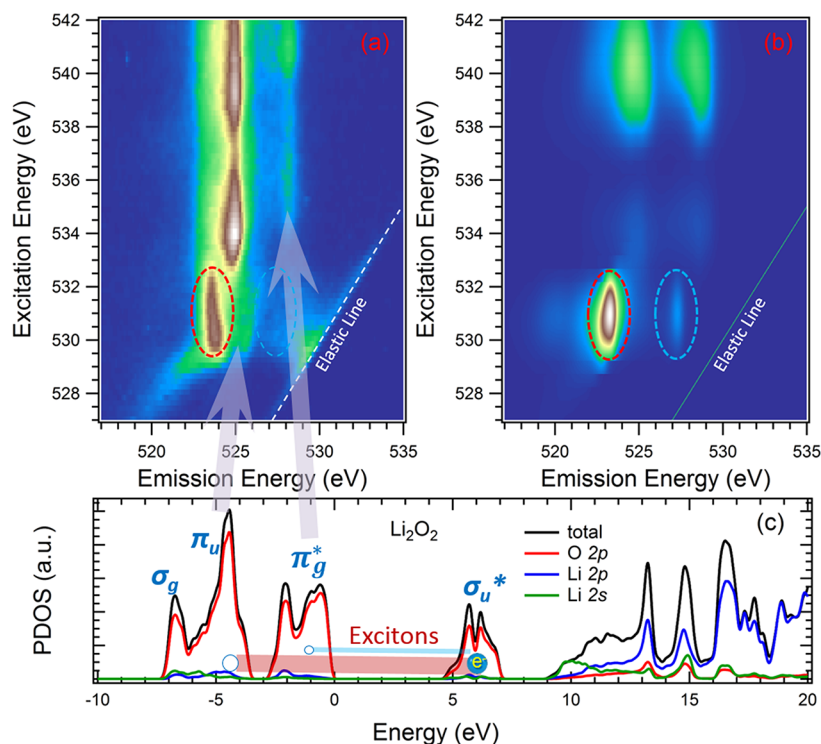


Figure 3. (a) Experimental O *K*-edge mRIXS of Li_2O_2 . A specific feature centered at 523.7 eV and two emission features at 525 and 528 eV emission energy are observed. (b) Calculated mRIXS of Li_2O_2 , which reproduces the experimental results with the striking feature at 523.7 eV emission energy (red circle). (c) Total and projected density of states of Li_2O_2 . Decay of the split valence band states lead to the two main emission features centered at 525 and 528 eV. However, the specific feature centered at 523.7 eV emission energy is from the excitations between the occupied and unoccupied O-2p states in the vicinity of the Fermi Level, due to the partially occupied O-2p states in peroxides.

unoccupied conduction band states that are further resolved by theoretical calculations.

Simulated mRIXS of Li_2O is displayed in Figure 1b with calculated total and projected density of states (pDOS) in Figure 1c. The calculated mRIXS reproduces the dominating features in the experimental results with an emission energy that agrees reasonably well with experiments. The weak feature at the bottom of the mRIXS map (about 530.8 eV excitation energy) is not reproduced in theory but resembles the absorption feature found in peroxides or O_2 ,^{14,35} indicating it is likely from impurity. Such a feature in peroxides will be elaborated below. pDOS plots show that O-2p states appear in the conduction band due to the hybridization with Li, sitting around 9 and 15 eV above the valence band maximum (VBM). These conduction band states correspond to the two excitation energy ranges around 534 and 540 eV in both sXAS (Figure S1) and mRIXS (Figure 1a) experiments. Furthermore, the filled O-2p states in Li_2O form a relatively narrow VB extending over only a 4 eV range below the VBM. Because the O- p_x , - p_y and - p_z orbitals in cubic Li_2O are equivalent, the VB lacks any splitting from anisotropic bonding. This explains the single dominating O-*K* emission line in mRIXS experiments, which corresponds to the decay from such a narrow VB to the core holes, as also shown in the theoretical mRIXS result in Figure 1b.

Compared with Li_2O , Li_2CO_3 is a more complex system and can be considered as a molecular solid with independent carbonate (CO_3^{2-}) ions surrounded by Li^+ ions. The mRIXS map Li_2CO_3 displays two main emission-line (without strong excitation energy dependence) features with several intensity packets in Figure 2a, centered at 521 (low intensity) and 526

eV (high intensity). Again, the main emission lines correspond to decays of VB electrons to the core holes, indicating there are obvious splitting of valence states in Li_2CO_3 . The well separated islands of mRIXS intensity at 533.7 eV excitation energy are again from sXAS-process, which is directly evidenced by the sXAS peak at the same excitation energy (Figure S2) and is known from the C = O bond of carbonates.^{4,5} The shift of the weak signals below 532 eV excitation energy in mRIXS is a typical Raman-like shift when excitation energy approaches the absorption edge.³⁶ The assignments and origins of the observed mRIXS features are further interpreted by mRIXS simulations (Figure 2b) and the density of states (Figure 2c). It is clear that C–O hybridization leads to the O-2p pDOS near the bottom of the CB, corresponding to the sXAS feature and mRIXS islands at 533.7 eV excitation energy. Meanwhile, O-2p pDOS near 12 eV result from Li–O hybridization, giving rise to the broad features at higher excitation energies. Compared with Li_2O , another major difference of the O 2p pDOS of Li_2CO_3 is the wide VB distribution over 8 eV range, with many peaks split in two groups separated by a gap of ~ 1.5 eV. The upper band is almost entirely composed of O-2p states while the lower band is a mix of O-2p and C-2p states (Figure 2c). The upper and lower VBs lead to two separated emission lines in the calculated mRIXS, centered respectively around 526 and 521 eV with the former being more intense than the latter. The split features at different emission energies are also reproduced (Figure 2b), consistent with experimental results. However, there is quantitative discrepancy between the experimental results and theoretical calculations on the energy values of the emission lines, especially in the lower excitation energy range.

This is traced to the choice of the U value in our DFT+ U calculations. As shown in the Supporting Information (Figure S4), although $U = 6$ eV is the optimal value for describing hole–polaron behavior in previous publications,^{33,34} decreasing the U value from 6 to 3 eV leads to a better quantitative agreement with experiments. In this context, GW³⁷ quasiparticle corrections to DFT or DFT+ U single-particle energies could be relevant to improving the predictive accuracy of first-principles BSE RIXS²⁸ approach. We also note that other theoretical method should be further explored for RIXS calculations; for example, a very recent theoretical work based on Wannier orbital method could reproduce the experimental results of Li_2CO_3 .³⁸

Therefore, all the mRIXS observations in Li_2O and Li_2CO_3 could be simulated and assigned to emission lines corresponding to the decay of VB electrons to the core holes generated during the sXAS process. The mRIXS contrast between the two systems is mainly due to the different VB configurations.

Figure 3 displays the experimental and theoretical mRIXS results of Li_2O_2 with a significantly changed DOS configuration due to the partially occupied O-2p bands. Li_2O_2 can be considered as a molecular solid comprised of independent O_2^{2-} peroxide ions surrounded by Li^+ ions. With the peroxo bond axis oriented along the c -axis of the Li_2O_2 crystal, bonding is highly anisotropic with O-2p states bifurcating into distinct π/π^* (p_x, p_y) and σ/σ^* (p_z) bonding/antibonding groups that are well separated in energy as shown in Figure 3c. The conduction band minimum in Li_2O_2 is essentially made up of unoccupied p_z orbitals oriented along the peroxo bond in σ_u^* symmetry.

Like Li_2CO_3 , the O-2p pDOS in the VBs of Li_2O_2 is distributed over a wide energy range and splits into regions with σ_g, π_u and π_g^* character with a gap of ~ 1 eV between the π_u and π_g^* states (Figure 3c). Therefore, two mRIXS emission-line features arise from the decay of electrons in the (σ_g, π_u) and π_g^* states to the core holes, leading to the two vertical mRIXS features at 525 and 528 eV emission energies (Figure 3a). Calculations based on VB decay again reproduce these emission-line features (Figure 3(b)). The feature at 525 eV emission energy is attributed to decays from the lower energy π_u states, while the 528 eV feature is attributed to decays from the π_g^* states. The excitation energy dependence of the mRIXS features are again consistent with the sXAS results (Figure S3), where broad features at 529–533.5 and 533–536 eV and above 538 eV are observed. The low excitation energy 529 to 533.5 eV sXAS feature corresponds to the special O–O bonding in Li_2O_2 ,¹³ i.e., the σ_u^* states from unoccupied p_z orbitals as explained above. Features above 538 eV excitation energy are from sXAS process to the high-energy Li–O hybridization states (Figure 3c). However, the broad feature in the intermediate excitation energies, 533 to 536 eV, has no corresponding pDOS, thus cannot be reproduced from theoretical calculations, but it matches almost exactly the strong feature of Li_2O (Figure 1). Our previous study has shown that Li_2O_2 could be degraded into Li_2O under soft X-ray exposure.¹⁴ We therefore assign the signals at 533 to 536 eV excitation energies to Li_2O from irradiation effect and/or impurity, even with our controlled and fast experimental scans.

The most striking finding of Li_2O_2 mRIXS is the intense feature near the 529 to 533.5 eV excitation and 523.7 eV emission energies, which appears as the strongest mRIXS feature in theoretical calculations (Figure 3b). As mentioned above, the sXAS signals at this energy range corresponds to the

unoccupied σ_u^* states from the O–O bonding in peroxides.¹⁴ However, the emission energy of this specific feature, 523.7 eV, is obviously different from the emission-line features (525 and 528 eV for Li_2O_2), indicating a different spectroscopic origin. More importantly, although with different broadening levels in excitation energy, the emission energy of this feature covers the oxygen redox mRIXS feature found in the battery electrodes with oxidized oxygen.^{13,17,18} It is therefore instructive and critical to analyze the character of this striking feature.

Parts a and b of Figure 4 show the density isosurface plots of the electron and hole contributions in our calculations that

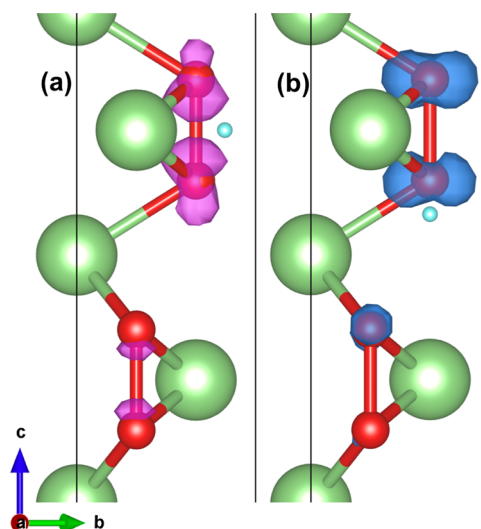


Figure 4. Density iso-surface plots of the electron (a) and hole (b) contributions within the excitonic wave function of the RIXS final state corresponding to the 523.7 eV emission mRIXS feature of Li_2O_2 . The blue (purple) shapes indicate the distributions of the holes (electrons) for plotting the electronic (hole) part of the two particle wave function. Green and red balls represent the lattice Li and O, respectively.

reproduces this 523.7 eV emission feature in theory. We choose the incoming photon polarization along the peroxo bond (p_z) direction and the outgoing polarization to be perpendicular to it, along p_x . Based on the incoming and outgoing photon energies, this mRIXS feature is reproduced successfully through a specific excitonic state, where the electron and hole has σ_u^* and π_u characters, respectively. As directly shown in Figure 4, the electron part of the excitonic wave function is composed of orbitals oriented along the peroxo bond axis, reflecting its p_z derived antibonding σ^* character. The hole density is formed predominantly from orbitals oriented along p_x orbitals with π bonding character. Therefore, the critical mRIXS feature at 523.7 eV emission and 529 to 533.5 eV excitation energy is an O-2p intraband excitation between the occupied π bonding states and the unoccupied σ^* antibonding states (Figure 3c). The mismatch between the energy difference of the excitonic states (Figure 3c) and experimental energy loss is mostly due to the core hole effect, which is accounted for in theoretical calculations that show consistent results to experiments (Figure 3b). We note that the mRIXS feature of Li_2O_2 is broader than the calculation results, and the O- K sXAS also shows a relatively broader peak compared with hard X-ray results (Figure S3),³⁰ therefore surface degradation/contamination of the Li_2O_2 at least partially contribute to the broadening of this particular

mRIXS feature. Dynamic disorders due to finite temperature may also contribute to the experimental broadening. It is important to note that, compared with the mRIXS feature of Li_2O_2 , the much sharper feature around the same emission energy in TM oxide based battery electrodes does imply differences in excitations and/or associated electron states, a topic that deserves further studies to clarify.

In summary, the mRIXS comparisons between the Li_2O_2 and $\text{Li}_2\text{O}/\text{Li}_2\text{CO}_3$ systems show clear spectroscopic differences between the response of (oxidized) O-2p in peroxides and the fully occupied 2p orbitals of the O^{2-} states. Theoretical calculations not only reproduce the mRIXS features, they also clarify that the specific Li_2O_2 mRIXS signals at 523.7 eV emission energy originates from O-2p intraband excitations, providing a spectroscopic signature for studying nonvalent oxygen state. The results suggest that the mRIXS feature found in battery electrodes with similar emission energy, but sharper excitation distribution,^{13,17,18} is not a feature from the decay of the occupied valence band electrons as claimed in previous publications. Instead, it indicates a specific excitation in highly oxidized TM oxide systems. However, it is important to note that one should not simply take this work as evidence of peroxides in battery electrodes. The excitations revealed here are inherent to highly oxidized systems, e.g., peroxides, superoxides, and even O_2 gas should all display excitonic features alike. Although no full-energy-range mRIXS results have been reported for other nonvalent oxygen compounds, a RIXS single spectrum of O_2 gas collected with 530.8 eV excitation energy did indicate a feature at 523.7 eV emission energy.³⁹ As discussed above, further works are still necessary to clarify the exact excitations responsible for the sharp mRIXS feature in electrodes based on TM oxides.^{13,17,18} Nonetheless, the results and analysis here conclude that the mRIXS feature at 523.7 eV emission energy emerges from specific excitations in highly oxidized systems, not from the decay of valence band electrons as indicated in previous works on battery electrodes. This clarification provides a critical foundation for further studies of the oxidized oxygen states in the more complex TM oxide systems, especially the electrochemical materials with oxygen redox activities.

■ ASSOCIATED CONTENT

Supporting Information

The Supporting Information is available free of charge on the ACS Publications website at DOI: 10.1021/acs.jpcllett.8b02757.

Detailed descriptions of the XAS and mRIXS experimental process and detailed descriptions of theoretical calculation methods. (PDF)

■ AUTHOR INFORMATION

Corresponding Authors

*(F.P.) E-mail: panfeng@pkusz.edu.cn.

*(T.P.D.) E-mail: tpd@stanford.edu.

*(W.Y.) E-mail: wlyang@lbl.gov.

ORCID

Chaitanya Das Pemmaraju: 0000-0002-9016-7044

John Vinson: 0000-0002-7619-7060

Yi-de Chuang: 0000-0002-2773-3840

Zahid Hussain: 0000-0002-6434-5134

Feng Pan: 0000-0002-8216-1339

Wanli Yang: 0000-0003-0666-8063

Author Contributions

[†]Z.Z. and C.D.P. contributed equally to this work.

Notes

The authors declare no competing financial interest.

■ ACKNOWLEDGMENTS

Advanced Light Source is supported by the Director, Office of Science, Office of Basic Energy Sciences, of the U.S. Department of Energy, under Contract No. DE-AC02-05CH11231. This work is also supported by Guangdong Innovation Team Project (No. 2013N080) and Shenzhen Science and Technology Research Grant (Peacock Plan KYPT20141016105435850). Theoretical work is supported by the US Department of Energy, Office of Science, Office of Basic Energy Sciences, Division of Materials Sciences and Engineering, under Contract No. DE-AC02-76SF00515. This research used resources of the National Energy Research Scientific Computing Center (NERSC), a U.S. Department of Energy Office of Science User Facility operated under Contract No. DE-AC02-05CH11231. Additionally, some of the computing for this project was performed on the Sherlock cluster, and support from Stanford University and the Stanford Research Computing Center is acknowledged. W.Y. would like to thank L. Andrew Wray (NYU) for thoughtful discussions.

■ REFERENCES

- (1) Chan, M. K. Y.; Shirley, E. L.; Karan, N. K.; Balasubramanian, M.; Ren, Y.; Greeley, J. P.; Fister, T. T. Structure of Lithium Peroxide. *J. Phys. Chem. Lett.* **2011**, *2*, 2483–2486.
- (2) Bruce, P. G.; Freunberger, S. A.; Hardwick, L. J.; Tarascon, J.-M. Li-O₂ and Li-S batteries with high energy storage. *Nat. Mater.* **2012**, *11*, 19–29.
- (3) Sathiyaa, M.; Rouse, G.; Ramesha, K.; Laissa, C. P.; Vezin, H.; Sougrati, M. T.; Doublet, M. L.; Foix, D.; Gonbeau, D.; Walker, W.; Prakash, A. S.; Ben Hassine, M.; Dupont, L.; Tarascon, J. M. Reversible anionic redox chemistry in high-capacity layered-oxide electrodes. *Nat. Mater.* **2013**, *12*, 827–835.
- (4) Qiao, R.; Lucas, I. T.; Karim, A.; Syzdek, J.; Liu, X.; Chen, W.; Persson, K.; Kostecki, R.; Yang, W. Distinct Solid-Electrolyte-Interphases on Sn (100) and (001) Electrodes Studied by Soft X-Ray Spectroscopy. *Adv. Mater. Interfaces* **2014**, *1*, 1300115.
- (5) Zhuo, Z.; Lu, P.; Delacourt, C.; Qiao, R.; Xu, K.; Pan, F.; Harris, S. J.; Yang, W. Breathing and oscillating growth of solid-electrolyte-interphase upon electrochemical cycling. *Chem. Commun.* **2018**, *54*, 814–817.
- (6) Xu, K. Nonaqueous Liquid Electrolytes for Lithium-Based Rechargeable Batteries. *Chem. Rev.* **2004**, *104*, 4303–4418.
- (7) McCalla, E.; Abakumov, A. M.; Saubanere, M.; Foix, D.; Berg, E. J.; Rouse, G.; Doublet, M. L.; Gonbeau, D.; Novak, P.; Van Tendeloo, G.; Dominko, R.; Tarascon, J. M. Visualization of O-O peroxo-like dimers in high-capacity layered oxides for Li-ion batteries. *Science* **2015**, *350*, 1516–1521.
- (8) Luo, K.; Roberts, M. R.; Hao, R.; Guerrini, N.; Pickup, D. M.; Liu, Y. S.; Edstrom, K.; Guo, J.; Chadwick, A. V.; Duda, L. C.; Bruce, P. G. Charge-compensation in 3d-transition-metal-oxide intercalation cathodes through the generation of localized electron holes on oxygen. *Nat. Chem.* **2016**, *8*, 684–91.
- (9) Seo, D.-H.; Lee, J.; Urban, A.; Malik, R.; Kang, S.; Ceder, G. The structural and chemical origin of the oxygen redox activity in layered and cation-disordered Li-excess cathode materials. *Nat. Chem.* **2016**, *8*, 692–697.
- (10) Grimaud, A.; Hong, W. T.; Shao-Horn, Y.; Tarascon, J. M. Anionic redox processes for electrochemical devices. *Nat. Mater.* **2016**, *15*, 121–126.

- (11) Assat, G.; Tarascon, J.-M. Fundamental understanding and practical challenges of anionic redox activity in Li-ion batteries. *Nat. Energy* **2018**, *3*, 373–386.
- (12) Suzuki, K.; Barbiellini, B.; Orikasa, Y.; Go, N.; Sakurai, H.; Kaprzyk, S.; Itou, M.; Yamamoto, K.; Uchimoto, Y.; Wang, Y. J.; Hafiz, H.; Bansil, A.; Sakurai, Y. Extracting the Redox Orbitals in Li Battery Materials with High-Resolution X-Ray Compton Scattering Spectroscopy. *Phys. Rev. Lett.* **2015**, *114*, 087401.
- (13) Yang, W.; Devereaux, T. P. Anionic and cationic redox and interfaces in batteries: Advances from soft X-ray absorption spectroscopy to resonant inelastic scattering. *J. Power Sources* **2018**, *389*, 188–197.
- (14) Qiao, R.; Chuang, Y.-D.; Yan, S.; Yang, W. Soft X-Ray Irradiation Effects of Li_2O_2 , Li_2CO_3 and Li_2O Revealed by Absorption Spectroscopy. *PLoS One* **2012**, *7*, e49182.
- (15) de Groot, F. M. F.; Grioni, M.; Fuggle, J. C.; Ghijsen, J.; Sawatzky, G. A.; Petersen, H. Oxygen 1s x-ray-absorption edges of transition-metal oxides. *Phys. Rev. B: Condens. Matter Mater. Phys.* **1989**, *40*, 5715–5723.
- (16) Firouzi, A.; Qiao, R.; Motallebi, S.; Valencia, C. W.; Israel, H. S.; Fujimoto, M.; Wray, L. A.; Chuang, Y. D.; Yang, W.; Wessells, C. D. Monovalent manganese based anodes and co-solvent electrolyte for stable low-cost high-rate sodium-ion batteries. *Nat. Commun.* **2018**, *9*, 861.
- (17) Gent, W. E.; Lim, K.; Liang, Y.; Li, Q.; Barnes, T.; Ahn, S. J.; Stone, K. H.; McIntire, M.; Hong, J.; Song, J. H.; Li, Y.; Mehta, A.; Ermon, S.; Tylliszczak, T.; Kilcoyne, D.; Vine, D.; Park, J. H.; Doo, S. K.; Toney, M. F.; Yang, W.; Prendergast, D.; Chueh, W. C. Coupling between oxygen redox and cation migration explains unusual electrochemistry in lithium-rich layered oxides. *Nat. Commun.* **2017**, *8*, 2091.
- (18) Xu, J.; Sun, M.; Qiao, R.; Renfrew, S. E.; Ma, L.; Wu, T.; Hwang, S.; Nordlund, D.; Su, D.; Amine, K.; Lu, J.; McCloskey, B. D.; Yang, W.; Tong, W. Elucidating anionic oxygen activity in lithium-rich layered oxides. *Nat. Commun.* **2018**, *9*, 947.
- (19) Léon, A.; Fiedler, A.; Blum, M.; Benkert, A.; Meyer, F.; Yang, W.; Bär, M.; Scheiba, F.; Ehrenberg, H.; Weinhardt, L.; Heske, C. Valence Electronic Structure of Li_2O_2 , Li_2O , Li_2CO_3 , and LiOH Probed by Soft X-ray Emission Spectroscopy. *J. Phys. Chem. C* **2017**, *121*, 5460–5466.
- (20) Qiao, R.; Li, Q.; Zhuo, Z.; Sallis, S.; Fuchs, O.; Blum, M.; Weinhardt, L.; Heske, C.; Pepper, J.; Jones, M.; Brown, A.; Spucses, A.; Chow, K.; Smith, B.; Glans, P.-A.; Chen, Y.; Yan, S.; Pan, F.; Piper, L. F. J.; Denlinger, J.; Guo, J.; Hussain, Z.; Chuang, Y.-D.; Yang, W. High-efficiency in situ resonant inelastic x-ray scattering (iRIXS) endstation at the Advanced Light Source. *Rev. Sci. Instrum.* **2017**, *88*, 033106.
- (21) Chuang, Y.-D.; Shao, Y.-C.; Cruz, A.; Hanzel, K.; Brown, A.; Frano, A.; Qiao, R.; Smith, B.; Domning, E.; Huang, S.-W.; Wray, L. A.; Lee, W.-S.; Shen, Z.-X.; Devereaux, T. P.; Chiou, J.-W.; Pong, W.-F.; Yashchuk, V. V.; Gullikson, E.; Reining, R.; Yang, W.; Guo, J.; Duarte, R.; Hussain, Z. Modular soft x-ray spectrometer for applications in energy sciences and quantum materials. *Rev. Sci. Instrum.* **2017**, *88*, 013110.
- (22) Vinson, J.; Rehr, J. J.; Kas, J. J.; Shirley, E. L. Bethe-Salpeter equation calculations of core excitation spectra. *Phys. Rev. B: Condens. Matter Mater. Phys.* **2011**, *83*, 115106.
- (23) Gilmore, K.; Vinson, J.; Shirley, E. L.; Prendergast, D.; Pemmaraju, C. D.; Kas, J. J.; Vila, F. D.; Rehr, J. J. Efficient implementation of core-excitation Bethe-Salpeter equation calculations. *Comput. Phys. Commun.* **2015**, *197*, 109–117.
- (24) Wu, J.; Sallis, S.; Qiao, R.; Li, Q.; Zhuo, Z.; Dai, K.; Guo, Z.; Yang, W. Elemental-sensitive Detection of the Chemistry in Batteries through Soft X-ray Absorption Spectroscopy and Resonant Inelastic X-ray Scattering. *J. Visualized Exp.* **2018**, DOI: 10.3791/57415.
- (25) Yang, W.; Liu, X.; Qiao, R.; Olalde-Velasco, P.; Spear, J. D.; Roseguo, L.; Pepper, J. X.; Chuang, Y.-d.; Denlinger, J. D.; Hussain, Z. Key electronic states in lithium battery materials probed by soft X-ray spectroscopy. *J. Electron Spectrosc. Relat. Phenom.* **2013**, *190*, 64–74.
- (26) Qiao, R.; Chin, T.; Harris, S. J.; Yan, S.; Yang, W. Spectroscopic fingerprints of valence and spin states in manganese oxides and fluorides. *Curr. Appl. Phys.* **2013**, *13*, 544–548.
- (27) Shirley, E. L. Theory and simulation of resonant inelastic X-ray scattering in s-p bonded systems: graphite, hexagonal boron nitride, diamond, and cubic boron nitride. *J. Electron Spectrosc. Relat. Phenom.* **2000**, *110–111*, 305–321.
- (28) Vinson, J.; Jach, T.; Müller, M.; Unterumsberger, R.; Beckhoff, B. Quasiparticle lifetime broadening in resonant x-ray scattering of NH_4NO_3 . *Phys. Rev. B: Condens. Matter Mater. Phys.* **2016**, *94*, 035163.
- (29) Farley, T. W. D.; Hayes, W.; Hull, S.; Hutchings, M. T.; Vrtis, M. Investigation of thermally induced Li + ion disorder in Li_2O using neutron diffraction. *J. Phys.: Condens. Matter* **1991**, *3*, 4761.
- (30) Chan, M. K. Y.; Shirley, E. L.; Karan, N. K.; Balasubramanian, M.; Ren, Y.; Greeley, J. P.; Fister, T. T. Structure of Lithium Peroxide. *J. Phys. Chem. Lett.* **2011**, *2*, 2483–2486.
- (31) Föppl, H. Die Kristallstrukturen der Alkaliperoxyde. *Z. Anorg. Allg. Chem.* **1957**, *291*, 12–50.
- (32) Zemann, J. Die Kristallstruktur von Li_2CO_3 . *Acta Crystallogr.* **1957**, *10*, 664–666.
- (33) Garcia-Lastra, J. M.; Myrdal, J. S. G.; Christensen, R.; Thygesen, K. S.; Vegge, T. DFT+U Study of Polaronic Conduction in Li_2O_2 and Li_2CO_3 : Implications for Li-Air Batteries. *J. Phys. Chem. C* **2013**, *117*, 5568–5577.
- (34) Erhart, P.; Klein, A.; Åberg, D.; Sadigh, B. Efficacy of the DFT + U formalism for modeling hole polarons in perovskite oxides. *Phys. Rev. B: Condens. Matter Mater. Phys.* **2014**, *90*, 035204.
- (35) Hennies, F.; Pietzsch, A.; Berglund, M.; Fohlsch, A.; Schmitt, T.; Strocov, V.; Karlsson, H. O.; Andersson, J.; Rubensson, J. E. Resonant inelastic scattering spectra of free molecules with vibrational resolution. *Phys. Rev. Lett.* **2010**, *104*, 193002.
- (36) Ament, L. J. P.; van Veenendaal, M.; Devereaux, T. P.; Hill, J. P.; van den Brink, J. Resonant inelastic x-ray scattering studies of elementary excitations. *Rev. Mod. Phys.* **2011**, *83*, 705–767.
- (37) Hybertsen, M. S.; Louie, S. G. Electron correlation in semiconductors and insulators: Band gaps and quasiparticle energies. *Phys. Rev. B: Condens. Matter Mater. Phys.* **1986**, *34*, 5390–5413.
- (38) Jia, C. A Wannier orbital based method for resonant inelastic x-ray scattering simulation. *arXiv:1810.02449*, 2018.
- (39) Glans, P.; Gunnelin, K.; Skytt, P.; Guo, J. H.; Wassdahl, N.; Nordgren, J.; Ågren, H.; Gel'mukhanov, F. K.; Warwick, T.; Rotenberg, E. Resonant X-Ray Emission Spectroscopy of Molecular Oxygen. *Phys. Rev. Lett.* **1996**, *76*, 2448–2451.